

# Specific heat in two-dimensional melting: supplemental material

(Dated: September 11, 2014)

The supplemental material contains further criteria for the melting temperature, details about the analysis of the specific heat, an illustration of the defect distribution at the specific heat peak, and a comment about the interaction parameter  $\Gamma$ .

## FINITE SIZE ANALYSIS OF THE TRANSLATIONAL ORDER

We have run simulations of the system with different sizes to check for finite size effects (periodic boundary conditions are used in all cases with a rectangular box). The simulations have shown that the transition points are almost unaffected, within the numerical uncertainties, and the peak of the specific heat reduces its height and widens, but does not move in  $\Gamma$ . This can be rationalized considering that long-wavelength fluctuations are absent in smaller systems, reducing the fluctuations. This result confirms the finding from the sub-box analysis of the experimental data presented below i.e. only the height of the peak is system dependent, but not its position with respect to the transition points.

On the other hand, a sub-box analysis of data with a fixed size can be used to obtain the transition points from fluid to hexatic, and from hexatic to crystal phases, independent from the analysis presented in the manuscript. Bagchi et al. proposed to use global order parameters calculated in subsystems with different lengths,  $L$ , which scales with different exponents in the isotropic fluid, hexatic fluid and crystal phases [1]. We study the scaling of the translational order parameter in the simulations,  $\Psi_T$ , to obtain an estimation of the hexatic-crystal transition, independent from the orientational correlation function,

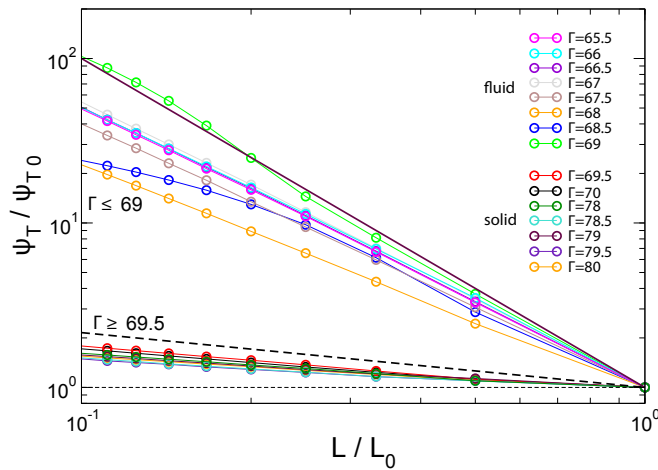


FIG. 1. Scaling of the translational order parameter for subsystems of size  $L$  for different values of  $\Gamma$ , as labeled in the graph. Both  $\Psi_T$  and  $L$  are normalized by the values of the whole system,  $\Psi_{T,0}$  and  $L_0$ . The continuous line shows  $L^{-2}$  and the broken one,  $L^{-1/3}$ .

as shown in Fig. 1 of the manuscript.  $\Psi_T$  is defined as  $\Psi_T = \langle |\frac{1}{N} \sum_k \exp \{i\mathbf{q}\mathbf{r}_k\}| \rangle^2$ , where  $\mathbf{q}$  is the wave-vector that maximizes the value of  $\Psi_T$  (the same value of  $\mathbf{q}$  is used for all states) and the summation runs over all particles in the system. The scaling of  $\Psi_T$  is presented in Fig. 1 for different states. It is clearly seen in the figure the sharp change from the behaviour of the liquid and hexatic states, with  $\psi_T \sim L^{-2}$ , to the crystal, where  $\psi_T \sim L^{-\eta_T}$ , with  $0 \leq \eta_T \leq 1/3$ , confirming the theoretical expectations, and also the transition point obtained from the analysis in the manuscript.

## 2D LINDEMANN PARAMETER

To further confirm the position of the transition points also for the experiment, we calculate the 2D modified Lindemann parameter

$$\gamma_L(\tau) = \langle (\bar{u}_i(\tau) - \bar{u}_j(\tau))^2 \rangle / 2a_0 \quad (1)$$

where  $\bar{u}_i(\tau)$  and  $\bar{u}_j(\tau)$  are the spatial displacements of particle  $i$  and a nearest neighbor particle  $j$  at time  $\tau$ , while the brackets denote an ensemble average. (In the analysis for the experiment, we used the center of mass of all nearest neighbors as a reference and not one neighboring particle. To locate the point of symmetry breaking, this makes no difference.) In the solid phase,  $\gamma_L(\tau)$  is finite for  $\tau \rightarrow \infty$  while in the hexatic and isotropic

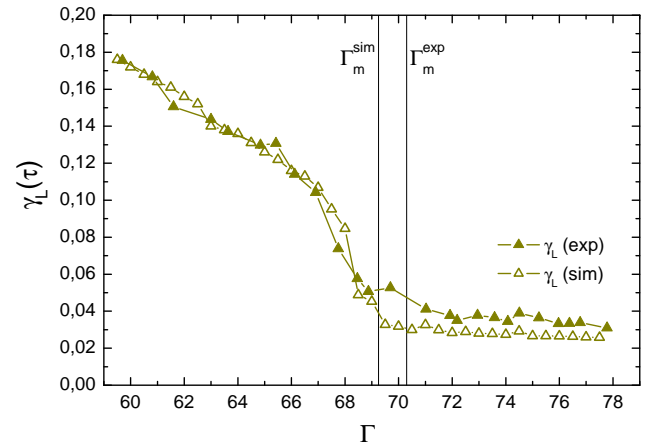


FIG. 2. Lindemann parameter  $\gamma_L(\tau = 3000 \text{ s})$  for experiment (filled symbols) and simulation (open symbols). The solid lines indicate the solid-hexatic transition temperatures for experiment and simulation.

fluid, it grows continuously for  $\tau \rightarrow \infty$  [2]. The results are shown in Fig. 2, where we choose  $\tau = 3000$  s and the corresponding number of simulation steps to indicate the long-time behaviour. For the simulation,  $\gamma_L$  stays constant above  $\Gamma_m^{sim} = 69.25$  (the solid-hexatic melting temperature) and increases rapidly afterwards. For the experiment, the increase is not that sharp as for the simulation. However it can be conducted that  $\gamma_L$  stays constant until  $\Gamma_m^{exp} \sim 70.3$  and increases afterwards first weakly and then more rapidly.

## ENERGY AND SPECIFIC HEAT

The specific heat at constant volume

$$\begin{aligned} C_V &= \left( \frac{\partial \langle E \rangle}{\partial T} \right)_V \quad (2) \\ &= -k_B \beta^2 \left( \frac{\partial \langle E \rangle}{\partial \beta} \right)_V = k_B \beta^2 \left( \frac{\partial^2 (\log Z)}{\partial \beta^2} \right)_V. \end{aligned}$$

with the mean (internal) energy  $\langle E \rangle = -\partial(\log Z)/\partial\beta$ , the partition function  $Z$  and  $\beta = 1/k_B T$ , can be given in terms of the energy fluctuations (see e.g. [3]),

$$\begin{aligned} \langle E^2 \rangle - \langle E \rangle^2 &= \frac{1}{Z} \frac{\partial^2 Z}{\partial \beta^2} - \left( \frac{1}{Z} \frac{\partial Z}{\partial \beta} \right)^2 \quad (3) \\ &= \frac{\partial}{\partial \beta} \left( \frac{1}{Z} \frac{\partial Z}{\partial \beta} \right) = \frac{\partial^2 (\log Z)}{\partial \beta^2}, \end{aligned}$$

leading to

$$C_V = \frac{\langle E^2 \rangle - \langle E \rangle^2}{k_B T^2}. \quad (4)$$

Since we have a purely repulsive system (with a single control parameter  $\Gamma$ ) in which pressure and volume can not be changed independently, we subscript the specific heat per particle as

$$c_N = \frac{\langle E^2 \rangle - \langle E \rangle^2}{N k_B T^2}. \quad (5)$$

For the usual approach (Eq. 2), we calculated the numerical derivative of the reduced energy  $\tilde{E} = \langle E \rangle / N k_B T$  in respect to  $\Gamma$ . With  $\partial T = -(T/\Gamma) \partial \Gamma$  it holds

$$\begin{aligned} c_N &= \frac{1}{N} \frac{\partial \langle E \rangle}{\partial T} = \frac{1}{N} \frac{\partial (\tilde{E} N k_B T)}{\partial T} \quad (6) \\ &= \dots = -k_B \Gamma^2 \frac{\partial (\tilde{E} / \Gamma)}{\partial \Gamma} = -\frac{\Gamma^2}{N} \frac{\partial (\langle E \rangle / T \Gamma)}{\partial \Gamma}. \end{aligned}$$

To demonstrate the equivalent energy scale in experiment and simulation, we show the average potential energy per particle and thermal energy

$$\langle E \rangle / N k_B T \quad (7)$$

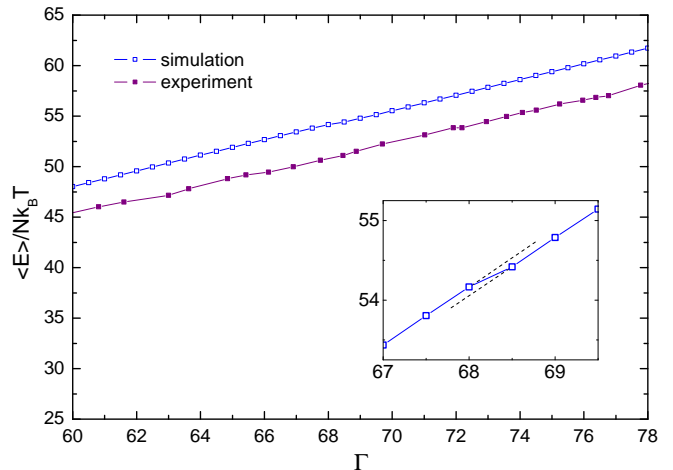


FIG. 3. Mean energy  $\langle E \rangle / N k_B T$  (per particle and thermal energy) for the experiment (filled symbols) and the simulation (open symbols). The inset shows a magnification for the simulation in the region of interest.

as a function of inverse temperature in Fig. 3. The difference between simulation and experiment is about 5% which we attribute to a demagnetization of particles in experiment due to the dipolar field of the neighboring particles which effectively reduces the outer field.

To be comparable, the cutoff value for the lattice summation is set to  $9a_0$  for both experiment and simulation where  $a_0$  is the average particle distance. The inset shows that there is only a single change of slope at  $\Gamma = 68$  to  $\Gamma = 68.5$  which leads to a single peak in the specific heat via the derivative approach (Fig. 4). The derivative of the internal energy (blue straight line in Fig. 4) exactly reproduces the peak in specific heat calculated from energy fluctuations for the simulations (blue dotted line in Fig. 4). In the experiment, however, the data scatters more compared to simulations. This experimental noise is attributed e.g. to fluctuations since the number of particles is not conserved exactly in the field of view and tiny density fluctuations snap through. Taking the derivative to calculate the specific heat per particle, any peak due to the phase transition(s) is beyond experimental resolution (Fig. 4 filled squares). Here, we would just like to show that the 'baseline' of the noise in  $c_N$  from experiment is comparable to the simulation data and agrees in the crystal side with the Dulong-Petit value.

## PEAK AND BASELINE LEVEL IN THE EXPERIMENT

In a system where a melting occurs due to an attractive interaction potential, energy fluctuations become large around the transition since both phases have typically a significant difference in density. For our two-dimensional system with a repulsive interaction potential, there is no

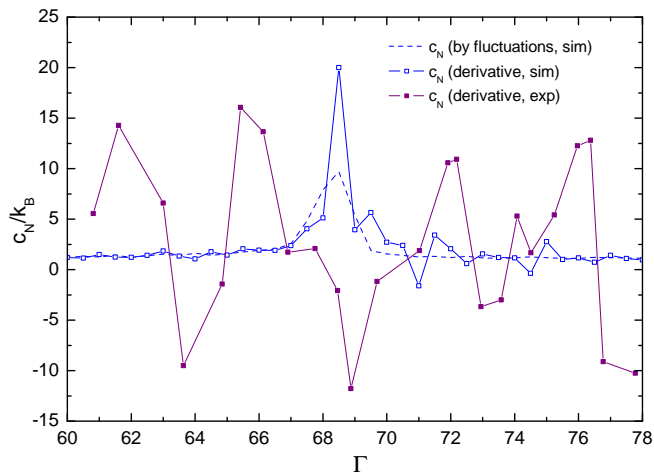


FIG. 4. Specific heat from energy fluctuations (dashed line, simulation) and derivative of internal energy (solid lines, simulation and experiment). For the experiments, the calculation from the derivative of the energy is too noisy and a reliable value can be obtained only from the energy fluctuations (see Fig.2b in the main manuscript).

change in density at all between the fluid and the solid phase when particle number is conserved. Just the mean particle distance is larger in the solid due to ordering which minimizes the potential energy. Thus, the peak in the specific heat is not caused by density fluctuations but by fluctuations in local order and structural rearrangements. In the given soft matter system, any fluctuations due to room temperature or mechanical vibrations lead directly to density fluctuations entering the internal energy beyond  $k_B T$ . Such perturbations increase the scale of energy fluctuations (right axis of Fig. 2b in the main manuscript) and unlike in simulations and the derivative approach, Dulong-Petit law is not recovered in the crystal. Nevertheless the susceptibility to perturbations is maximized at the phase transition (dislocation unbinding) which affects the peak height in the specific heat but the peak position at  $\Gamma_{c_N} = 68.5$  is not affected (Fig. 2b of the main manuscript).

### CUTOFF DEPENDENCY

The energy per particle is calculated up to a cutoff distance. In the experiment where we do not have periodic boundary conditions, this cutoff value reduces the effective field of view, given that the energy summation can be taken within the same cutoff value for every particle. A large cutoff value increases the statistics for every particle whereas a small cutoff value increases the statistics of the number of particles. Fig. 5 shows the specific heat per particle as a function of  $\Gamma$  for different cutoff values of  $5a_0$ ,  $9a_0$  (as used in simulation),  $15a_0$ , and  $20a_0$ . In Fig.2b of the main manuscript we took a cutoff value of

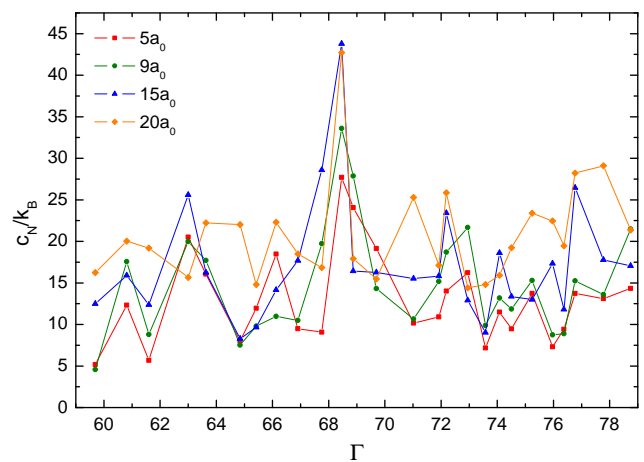


FIG. 5. Experimental specific heat from energy fluctuations, with the energy calculated with different cutoffs, as labeled. Note that the peak decreases with decreasing interaction range.

$15a_0$ . Note that if the cutoff value is too small, the peak vanishes.

### SPECIFIC HEAT PEAK AND DEFECT CORE ENERGY

The peak height of the specific heat in Fig. 2a of the main manuscript is about  $20k_B$ . A rough estimate for the peak height is given by the number of dislocations which dissociate in a small temperature range times the core energy of the dislocations. The core energy of *isolated* dislocations is approximately  $5.5k_B T$  in the hexatic phase above  $T_m$  [4]. We note the change of the overall defect density  $\rho$ . Between  $\Gamma = 68.5$  to  $\Gamma = 68$  the change in defect density is  $\Delta\rho \approx 0.1$  which corresponds to a change in defect number of  $\Delta N_{def} \approx 200$ . We then observe

$$c_N \approx \frac{5.5k_B T}{2N} \frac{\Delta N_{def}}{\Delta T} = -\frac{5.5k_B \Gamma}{2N} \frac{\Delta N_{def}}{\Delta \Gamma} \approx 30k_B$$

(The factor of 1/2 comes due to the fact that a dislocation consists of two defects.) This value is already larger than the measured one which implies that the core energy is overestimated.

Fig 6 shows a snapshot for the experimental system at  $\Gamma = 68.4$  where the specific heat peaks. Particles with six nearest neighbors are marked with open circles, fivefold coordinated sites with green and sevenfold coordinated sites with orange filled circles. Isolated dislocations which count in the analysis of Fig. 2c,d in the manuscript are illustrated with smaller black dots (isolated dislocations might be cut by the field of view). Most of the defects are arranged in clusters, only 20% appear as isolated dislocations. This is beyond KTHNY theory where a dilute gas of dislocations is assumed for renormalization procedure. If the defect density increases, the clustering is

quite natural since the dislocations as well as the disclinations have an attractive interaction [4]. This implicitly means that the fugacity is locally increased in the cluster or equivalently that the core energy is locally reduced ( $< 5.5k_B T$ ). This behavior has already been observed for geometrical defects like interstitials and vacancies where the fugacity of dislocations is increased locally, too [5]. Note, that all clusters consist of the same number of five- and seven-folded particles and may be interpreted as dislocation clusters. Isolated disclinations or clusters of disclinations (with unequal number of five- and seven-folded particles) are *not* found in the hexatic phase but only in the isotropic phase with the isolated disclinations being less than 5‰ (Fig 2b of the main manuscript).

Since we know implicitly that the core energy of clustered defects is overestimated we restrict to isolated dislocations in the assessment of the specific heat due to defects. In Fig. 2c and Fig. 2d, a hyperbolic tangent functional form is fitted to the defect densities of experiment and simulations to get a smooth derivative. The

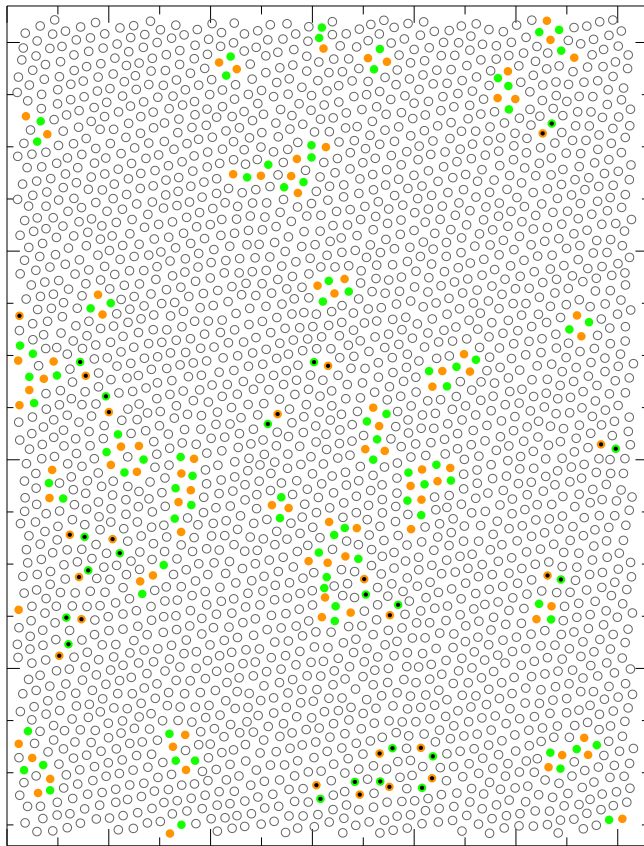


FIG. 6. Snapshot of the experimental system at  $\Gamma = 68.4$  where the specific heat peaks. Particles with six nearest neighbors are marked with open circles, fivefold coordinated sites with green and sevenfold coordinated sites with orange filled circles. Isolated dislocations are illustrated with smaller black dots (isolated dislocations might be cut by the field of view).

peak of the derivative (red curve in Fig 2c,d) gives the contribution of the two distinct species of isolated defects. The peak positions of isolated dislocations is already shifted within the hexatic phase, well separated from the melting temperature  $\Gamma_m$ . Of course, all defects contribute to the specific heat: adding clustered dislocations and disclinations shifts the peak to even higher temperatures (lower  $\Gamma$ ) but it can not be attributed to the onset of disclination unbinding, since the disclination density times disclination core energy is too small: a rough estimate of the disclination core energy ( $\approx 5k_B T$ ) times the number of unbinding disclinations ( $\approx 1\%$  at  $\Gamma = 58 \pm 1$ ) gives  $\approx 1k_B$ .

### DETERMINATION OF THE MAGNETIC PARTICLE SUSCEPTIBILITY

To determine the exact interaction strength, the magnetic susceptibility  $\chi$  has to be measured for every colloidal batch. In [6, 7] this was done via a comparison of the pair correlation function  $g(r)$  of the experimental system and by computer simulations from J. M. Mendez-Alcaraz in the isotropic fluid phase. With the given  $\chi$ , melting was found between  $69.5 < \Gamma_m < 62.5$  [8]. In [4, 9–11] melting was found at  $\Gamma_m = 60.5 \pm 0.5$  and the second transition at  $\Gamma_i = 57 \pm 0.5$ . The susceptibility was further determined with SQUID measurements being consistent with the previous values but with large error bars. In the present manuscript as well as in [14] the experimental melting transition is found to be at  $\Gamma_m = 70.2 \pm 0.3$  if the magnetic susceptibility is again determined via comparison of pair correlation functions  $g(r)$  with simulations of a) J. M. Mendez-Alcaraz [6], b) D. Hajnal [12, 13], and c) T. Kruppa [14] and d) A.M. Puertas independently. However, the transition temperatures are just scaled with a constant factor compared to previous ones and the agreement in the present manuscript with transition temperatures from simulation is excellent. We attribute the changes to the increased resolution of CCD-cameras and digital image processing compared to those a decade ago.

- 
- [1] K. Bagchi, H. C. Andersen, Phys. Rev. Lett. **76**, 255 (1995).
  - [2] V. M. Bedanov, G. V. Gadiyak, Phys. Lett. **109A**, 289 (1985); X. H. Zheng, J. C. Earnshaw, Europhys. Lett. **41**, 635 (1998).
  - [3] P. M. Chaikin and T. C. Lubensky, *Principles of Condensed Matter Physics* (Cambridge University Press, Cambridge, England, 1995), Chap. 3, p. 120.
  - [4] C. Eisenmann, U. Gasser, P. Keim, G. Maret, H. H. von Grünberg, Phys. Rev. Lett. **95**, 185502 (2005).
  - [5] David Polster, PhD-thesis: <http://nbn-resolving.de/urn:nbn:de:bsz:352-268915>

- [6] K. Zahn, J. M. Mendez-Alcaraz, G. Maret, Phys. Rev. Lett., **79**, 175 (1997)
- [7] K. Zahn, R. Lenke, G. Maret, Phys. Rev. Lett. **82**, 2721 (1999)
- [8] K. Zahn, G. Maret, Phys. Rev. Lett. **85**, 3656 (2000)
- [9] P. Keim, G. Maret, U. Herz, H. H. von Grünberg, Phys. Rev. Lett. **92**, 215504 (2004)
- [10] H. H. von Grünberg, P. Keim, K. Zahn, G. Maret, Phys. Rev. Lett. **93**, 255703 (2004)
- [11] P. Keim, G. Maret, and H. H. von Grünberg, Phys. Rev. E **75**, 031402 (2007).
- [12] D. Hajnal, J. Brader, R. Schilling, Phys. Rev. E, **80**, 021503 (2009)
- [13] D. Hajnal, M. Oettel, R. Schilling, Jour. of Non-Cryst. Sol. **357**, 302 (2011)
- [14] S. Deutschländer, T. Kruppa, H. Löwen, G. Maret, and P. Keim, Phys. Rev. Lett. **111**, 098301 (2013)